A Contribution to Wavelet-Based Subgrid Modeling

Ulf Andersson* Björn Engquist† Gunnar Ledfelt*
Olof Runborg*

Abstract

A systematic technique for the derivation of subgrid scale models in the numerical solution of partial differential equations, is described. The technique is based on Haar wavelet projections of the discrete operator followed by a sparse approximation. As numerical testing suggests, the resulting numerical method will accurately represent subgrid scale phenomena on a coarse grid. Applications to numerical homogenization and wave propagation in materials with subgrid inhomogeneities are presented.

1 Introduction

In the numerical simulation of partial differential equations, the existence of subgrid scale phenomena poses considerable difficulties. With subgrid scale phenomena, we mean processes which should influence the solution on the computational grid but which have length scales shorter than the grid size. Fine scales in the initial values may for example interact with fine scales in the material properties and produce coarse scale contributions to the solution.

There are many traditional ways to deal with this problem. Local mesh refinement is useful in several applications. A drawback with this method is that it might lead to reflections at mesh size discontinuities, increased complexity of the algorithm and reduced time steps for explicit methods due to stability constraints. There also exist a number of methods based on physical considerations for a specific application such as turbulence models in computational fluid dynamics, [16], and analytically derived local subcell models in computational electromagnetics, [15]. Another example is the immersed interface method, [13] used on Cartesian grids. In this method the subgrid variations of the shape of a material interface is taken into consideration by changing the updating stencils near the interfaces. Shock tracking or shock fitting can also be seen as subgrid models, [1].

*Numerical Analysis and Computing Science, KTH

†Numerical Analysis and Computing Science, KTH and Department of Mathematics UCLA. Research supported by the grants ARPA/ONR, N00014-92-J-1890, ONR, N00014-91-J-1034, NSF, DMS-91-03104.

In this paper we present a general procedure for constructing subgrid models to be used on a coarse grid where the smallest scales are not resolved. The objective is to find models that accurately reproduce the effect of subgrid scales and that in some sense are similar to the original differential operator. The starting point is a finite-dimensional approximation of a differential equation, $Lu = f$, where L approximates the operator and u the solution. The operator L can be written on the form

$$L = P(\Delta, A, h), \tag{1}$$

where Δ is a collection of difference operators, A are discretized variable coefficients, typically diagonal matrices, and h represents the grid size, which is assumed to be sufficiently small to resolve all scales. We seek an operator $\bar{L}$ and a right hand side $\bar{f}$ with the following properties. First, $\bar{L}\bar{u} = \bar{f}$ and $\bar{u}$ is a projection of u onto a lower dimensional subspace. Second, $\bar{L}$ can be written on the same form as L,

$$\bar{L} = P(\Delta, H, \bar{h}), \tag{2}$$

but with $\bar{h} \gg h$ and the structure of H close to the structure of A, typically diagonal dominant and sparse. We interpret H as the subgrid model of A. If A corresponds to a material coefficient, H can be seen as the effective material coefficient. The procedure outlined above resembles that of *homogenization*, the classical analytic technique used for a large class of these problems in the continuous case. In view of this, we will call $\bar{L}$ the homogenized operator. See Bensoussan et al., [3], for a thorough description of homogenization.

Our method is based on multiresolution analysis with wavelet projections and approximation of the discrete operator. Although it can be used with any type of discretization—it is algebraic and only deals with a linear system of equations—we envisage that it will be most useful for computations on Cartesian grids. A subgrid model would mitigate the main drawback of Cartesian grids, their poor ability to describe geometry accurately. It will still allow a solver to capitalize on their advantages, computational speed and small errors due to artificial dispersion and reflections. Typical applications would be oil reservoir simulations and computational electromagnetics. With this paper we want to give a proof of concept that the technique produces useful H. Maximum efficiency in the computation of H has not been our main concern. Since H is supposed to be reused, either in multiple computation with different initial data, or in multiple places within the computational domain, efficiency is often of secondary importance. Moreover, H itself can be of interest in the analysis of a physical problem.

The great advantage of this procedure to derive subgrid models is its generality. It can be used on any system of differential equations and does not require separation into the distinct $\mathcal{O}(\epsilon)$ and $\mathcal{O}(1)$ scales or periodic coefficients. It can also be used to test if it is physically reasonable to represent fine scales effects on a coarse scale grid with a local operator.

This work is a continuation of the work by Dorobantu and Engquist, [8], and based on ideas from Brewster and Beylkin, [5]. See also [10] for analysis

in the one-dimensional case. Moreover, there are similarities with numerical homogenization based on techniques from algebraic multigrid, [12, 14] and from the use of special purpose finite element methods, [11]. In this paper we extend the method in [8] to hyperbolic problems and introduce new truncation algorithms. This truncation can also be used for compression of the wavelet based representation of Calderon-Zygmund operators in [5].

The paper is organized as follows. In Section 2 we give the mathematical background and in Sections 3 and 4 we study elliptic and hyperbolic model problems respectively and present a number of numerical examples. The examples cover random and localized inhomogeneities. In one example with the 2D Helmholtz equation, we show that the effect of a small geometric detail can be captured on a coarse grid.

2 Wavelet Projection of Difference Operators

We will develop our subgrid scale models within the framework of wavelet based multiresolution analysis in the standard Haar basis. Numerical tests have not shown any substantial advantage with using more sophisticated wavelets. For a detailed description of multiresolution analysis, see e.g. [7].

2.1 Wavelet projections

Given the full discrete solution operator on a fine grid we wish to find an operator of lower dimension that extracts only the coarse scales of the solution. Let V_j and W_j refer to the usual scaling and wavelet spaces of the Haar system. Then, for a solution in $V_{j+1} = V_j \oplus W_j$, the coarse scale is represented by V_j, and we are thus interested in the operator that yields the solution's projection onto V_j.

Consider the equation

$$L_{j+1}U = F, \qquad U, F \in V_{j+1}, \tag{3}$$

originating from a discretization of a differential equation, where U is identified as a piecewise constant approximation of $u(x)$, the solution to the continuous problem. We introduce the orthogonal transformation

$$\mathcal{W}_j : V_{j+1} \to W_j \times V_j, \quad \mathcal{W}_j U \equiv \begin{bmatrix} U_h \\ U_l \end{bmatrix} \qquad U_h \in W_j, \qquad U_l \in V_j, \tag{4}$$

and note that the linear operator $\mathcal{W}_j L_{j+1} \mathcal{W}_j^\top$ can be decomposed into four operators $L_{j+1} = A_j + B_j + C_j + L_j$, acting between the subspaces V_j and W_j, such that (3) becomes

$$\begin{bmatrix} A_j & B_j \\ C_j & L_j \end{bmatrix} \begin{bmatrix} U_h \\ U_l \end{bmatrix} = \begin{bmatrix} F_h \\ F_l \end{bmatrix}, \qquad U_h, F_h \in W_j, \qquad U_l, F_l \in V_j. \tag{5}$$

when we apply $\mathcal{W}_j$ from the left. Block Gaussian elimination now gives an equation for U_l, the coarse part of the solution,

$$\bar{L}_j U_l = \bar{F}_j, \quad \bar{L}_j = L_j - C_j A_j^{-1} B_j, \quad \bar{F}_j = F_l - C_j A_j^{-1} F_h. \tag{6}$$

Hence, our new "coarse grid operator" $\bar{L}_j$ is the Schur complement of $\mathcal{W}_j L_{j+1} \mathcal{W}_j^\top$. We also get the homogenized right hand side, $\bar{F}_j$.

For higher dimensions, a standard tensor product extension of the multiresolution analysis allows us to use essentially the same derivation as above to obtain coarse grid operators.

Before we go on we should note that in general $\bar{L}_j$ will not be sparse even if L_{j+1} is. For the method to be efficient we must be able to approximate $\bar{L}_j$ with a *sparse* matrix. In Section 2.3 below we will get back to this issue and we will in subsequent sections show that this can indeed be done.

The homogenization procedure can be applied recursively on $\bar{L}_j$ to get $\bar{L}_{j-1}$ and so on. This can easily be verified when L_{j+1} is symmetric positive definite. Furthermore, the condition number will not deteriorate. From [2], Chapter 3 with $L_{j+1} = L_{j+1}^T$ and

$$c_1 ||U||^2 \leq \langle L_{j+1} U, U \rangle \leq c_2 ||U||^2, \qquad \forall U \in \mathbb{R}^{2^{j+1}} \tag{7}$$

we have with the same constants c_1, c_2,

$$c_1 ||V||^2 \leq \langle \bar{L}_j V, V \rangle \leq c_2 ||V||^2, \qquad \forall V \in \mathbb{R}^{2^j}, \tag{8}$$

where $\bar{L}_j$ is defined by (6) and $\langle u, v \rangle = \sum_k \bar{u}_k v_k$. For the first step in the process an improvement in the condition number can often be estimated from

$$\begin{aligned} \langle \bar{L}_j V, V \rangle &= \langle (L_j - B_j^T A_j^{-1} B_j) V, V \rangle = \langle L_j V, V \rangle - \langle A_j^{-1} B_j V, B_j V \rangle \\ &\leq \langle L_j V, V \rangle. \end{aligned} \tag{9}$$

Typically for standard discretizations $\max_{||V||=1} \langle L_j V, V \rangle < \max_{||U||=1} \langle L_{j+1} U, U \rangle$. Note also that $\bar{L}_j$ remains symmetric and, in the Haar case, lower triangular if L_{j+1} has these properties.

In some important cases the homogenized operator has been proven to remain in the same form as the original operator. In [8] it was shown that with standard discretization the one-dimensional elliptic operator $-(au_x)_x$ will preserve its discrete divergence form during homogenization. More precisely,

$$L_{j+1} = \frac{1}{h^2} \Delta_+ \mathrm{diag}(a) \Delta_- \qquad \Rightarrow \qquad \bar{L}_j = \frac{1}{h^2} \Delta_+ H_j \Delta_-, \tag{10}$$

where the subgrid model H_j is a strongly diagonal dominant matrix. Analogously, for the first order operator au_x and the two dimensional elliptic operator $-\nabla \cdot (a \nabla u)$, the discretized form is preserved during homogenization, although in the latter case cross-derivatives must also be included.

2.2 Comparison with homogenization

Homogenization is a classical analytical way to approximate the effect of some classes of periodic or stochastic subcell scales. The problem is often formulated

as follows. Consider a set of operators L_ϵ, indexed by the small parameter ϵ, and a right hand side f. Find the *homogenized operator* $\bar{L}$ defined by

$$L_\epsilon u_\epsilon = f, \qquad \lim_{\epsilon \to 0} u_\epsilon = \bar{u}, \qquad \bar{L}\bar{u} = f. \tag{11}$$

In certain cases the convergence above and existence of the homogenized operator can be proved, [3].

For simple model problems, with coefficients periodic on the fine scale, exact closed form solutions can be obtained. For instance, with $a(y)$ positive, one-periodic and bounded away from zero, we have the one-dimensional examples

$$L_\epsilon = -\frac{\partial}{\partial x}\left(a(x/\epsilon)\frac{\partial}{\partial x}\right), \qquad \bar{L} = -\bar{a}\frac{\partial^2}{\partial x^2}, \qquad \bar{a} = \left(\int_0^1 \frac{dy}{a(y)}\right)^{-1}, \tag{12}$$

and, with the same $\bar{a}$,

$$L_\epsilon = \frac{\partial}{\partial t} + a(x/\epsilon)\frac{\partial}{\partial x}, \qquad \bar{L} = \frac{\partial}{\partial t} + \bar{a}\frac{\partial}{\partial x}. \tag{13}$$

The model examples (12) and (13) are used in Sections 3 and 4 respectively.

In higher dimensions, the solution to (11) is a little more complicated, although for model problems the structure of the homogenized operator can still be written down, as long as the coefficients are periodic. In the d-dimensional elliptic case, let $A(y) \in \mathbb{R}^{d\times d}$ be one-periodic in each of its arguments and let I_d denote the unit square. It can then be shown, [3], that

$$L_\epsilon = -\nabla\cdot(A(\frac{x}{\epsilon})\nabla), \quad \bar{L} = -\nabla\cdot(H\nabla), \quad H = \int_{I_d} A(y) - A(y)D\chi(y)dy, \tag{14}$$

where $D\chi$ is the jacobian of the vector valued function $\chi(y) \in \mathbb{R}^d$, whose components χ_k are given by solving the so called cell problems

$$\nabla\cdot(A(y)\nabla\chi_k) = \sum_{i=1}^{d} \frac{\partial}{\partial y_i} a_{ik}(y), \qquad k = 1, \ldots, d, \tag{15}$$

with periodic boundary conditions for χ_k. Note that H is a constant matrix. See [9] for a practical application of this.

There is a striking relationship between the analytically homogenized operator in (14) and the the Schur complement $\bar{L}_j$ in (6). The first term in both the expressions represent averaged operators, L_j in a discrete sense and $\int_{I_d} A$ in an integral sense. In both formulations a correction term is subtracted from the average. Furthermore, in the correction term χ is the solution of an elliptic equation and A_j^{-1} is a discrete positive definite solution operator.

In the classical homogenization setting (14) homogenization gives the asymptotic expansion

$$u_\epsilon(x) = \bar{u}(x) + \epsilon u_1(x, x/\epsilon) + \mathcal{O}(\epsilon^2) \tag{16}$$

for the solution, see [3]. The techniques described in [11], [12] and [14] give homogenized operators with coarse grid solutions which directly samples (16). The oscillatory term $\epsilon u_1(x, x/\epsilon)$ is contained in the solution. In the wavelet homogenization the solution is a projection of u_ϵ onto a coarse scale V_j space. The influence of the u_1 term, which oscillates with mean zero [3], is then significantly reduced.

2.3 Compact representation of projected operators

When the operator L_{j+1} is derived from a finite difference, finite element or finite volume discretization, it is sparse and of a certain structure. In one dimension it might for instance be tridiagonal. However, as remarked in Section 2.1, the matrix $\bar{L}_j$ is not sparse since A_j^{-1} is usually dense. Computing all components of $\bar{L}_j$ would be inefficient. Fortunately, $\bar{L}_j$ will be diagonal dominant in many important cases. For instance, in [8] it is proved that for a class of elliptic problems the matrix elements of $\bar{L}_j$ decay exponentially away from the diagonal. We should then be able to find a sparse matrix that is a close approximation of $\bar{L}_j$.

One simple way to approximate $\bar{L}_j$ is to set all components outside a prescribed bandwidth equal to zero. Let us define *truncation* of M to bandwidth ν as

$$\text{trunc}(M, \nu)_{ij} = \begin{cases} M_{ij}, & \text{if } 2\,|i-j| \leq \nu - 1 \\ 0, & \text{otherwise.} \end{cases} \tag{17}$$

This procedure was introduced in [4] and used in [8]. We propose that $\bar{L}_j$ be projected onto banded form in a more effective manner. Let $\{\boldsymbol{v}_j\}_{j=1}^{\nu}$ be a set of linearly independent vectors in $\mathbb{R}^{2^j}$. We define the *band projection*, $\text{band}(M, \nu)$, of a matrix M as the projection of M onto the subspace of matrices with bandwidth ν such that

$$M\boldsymbol{x} = \text{band}(M, \nu)\boldsymbol{x}, \qquad \forall \boldsymbol{x} \in \text{span}\{\boldsymbol{v}_1, \boldsymbol{v}_2, \ldots, \boldsymbol{v}_\nu\}. \tag{18}$$

In our setting M will usually operate on vectors representing smooth functions, for instance solutions to elliptic equations, and a natural choice for the $\boldsymbol{v}_j$ vectors are thus the first ν polynomials,

$$\boldsymbol{v}_j = \{1^{j-1}, 2^{j-1}, \ldots, N^{j-1}\}^T. \tag{19}$$

For the case $\nu = 1$ we should remark that we get the standard "masslumping" of a matrix, often used in the context of finite element methods.

This technique is similar to the probing technique used by Chan et al., [6]. In that case the vectors $\boldsymbol{v}_j$ are sums of unit vectors. Other probing techniques have been suggested by Axelsson, Pohlman and Wittum, see e.g. Chapter 8 in [2]. The choice of $\boldsymbol{v}_j$ vectors could be optimized if there is some a priori knowledge of the homogenized solution. In some cases the band projection technique only gives improvements for small values of ν, see Figure 1. The probing technique

of [6] could be used for larger ν in our examples. Numerical evidence indicate that for small values of ν, the band projection technique is more efficient.

The focus in this paper is on the principle and the truncation $\mathrm{trunc}(\bar{L}_j, \nu)$, is done after computing the full inverse of A_j. In large scale applications, to be reported elsewhere, incomplete or thresholded LU-decomposition will be used. The computation of $\mathrm{band}(\bar{L}_j, \nu)$ can be based on $\mathrm{trunc}(\bar{L}_j, \mu)$, $\mu > \nu$. The additional computational cost is proportional to $(\nu^3 + \mu\nu)N$. The $\nu^3 N$ term corresponds to solving N $\nu \times \nu$ systems and $\mu\nu N$ to computing the right hand sides, see also [2].

The truncation methods described above are even more efficient when applied to the subgrid model H_j instead of directly to the homogenized operator. The following proposition shows that when the solution to the homogenized problem belongs to the Sobolev space H_1, the accuracy is one order higher.

Proposition 1 *Suppose $L = \Delta_+ H \Delta_-$ and $LU = h^2 f$. Let $\kappa = ||L^{-1}|| \cdot ||H||$ and*

$$r = \frac{||\delta L||}{||L||} = \frac{||\delta H||}{||H||} < \frac{1}{4\kappa}, \tag{20}$$

where $||\cdot||$ denotes the l_2-norm. Furthermore, let u be any H_1-function such that $U_j = u(jh)$. Then, if

$$(L + \delta L)(U + \delta U_L) = \Delta_+ (H + \delta H)\Delta_- (U + \delta U_H) = h^2 f \tag{21}$$

the following bounds on the perturbed solutions hold $\forall f$

$$||\delta U_L|| \leq \frac{4r\kappa}{1 - 4r\kappa}||U||, \tag{22}$$

$$||\delta U_H|| \leq \frac{1}{2} \cdot \frac{4r\kappa}{1 - 4r\kappa}||\Delta_- U|| \leq \frac{h}{2} \cdot \frac{4r\kappa}{1 - 4r\kappa}||u||_{H_1}. \tag{23}$$

The bound (22) is sharp.

Proof: Using $||\Delta_+|| = ||\Delta_-|| = 2$ and (20) we have

$$||L^{-1}\delta L|| \leq \frac{||L^{-1}|| \cdot ||\delta H|| \cdot ||\Delta_+ H \Delta_-||}{||H||} \leq 4r||L^{-1}|| \cdot ||H|| = 4r\kappa < 1. \tag{24}$$

Therefore,

$$||\delta U_L|| = ||(I + L^{-1}\delta L)^{-1} L^{-1}\delta L U|| \leq \frac{||L^{-1}\delta L||}{1 - ||L^{-1}\delta L||}||U|| \leq \frac{4r\kappa}{1 - 4r\kappa}||U||, \tag{25}$$

proving the first bound. In the second case,

$$||L^{-1}\Delta_+ \delta H \Delta_-|| \leq 4||L^{-1}|| \cdot ||\delta H|| \leq 4r\kappa < 1, \tag{26}$$

giving

$$\begin{aligned} ||\delta u_H|| &= ||(I + L^{-1}\Delta_+\delta H\Delta_-)^{-1}L^{-1}\Delta_+\delta H\Delta_- U|| \\ &\leq \frac{||L^{-1}\Delta_+\delta H||}{1 - ||L^{-1}\Delta_+\delta H\Delta_-||}||\Delta_- U|| \leq \frac{2r\kappa}{1-4r\kappa}||\Delta_- U|| \end{aligned} \tag{27}$$

which proves the second bound. The choice $L = -\Delta_+\Delta_-$, $\delta L = -rI||L||$ and f the eigenvector of L corresponding to its smallest eigenvalue shows the sharpness of (22). The final step, $||\Delta_- U|| \leq h||u||_{H_1}$, follows from Cauchy-Schwarz' inequality. Note that (22) cannot be improved to $\mathcal{O}(h)$ by replacing $||U||$ with $||u||_{H_1}$. □

In two dimensions truncation to banded form is not adequate, since the truncated operator will not be close to the exact operator, which will be block banded. However, both the crude truncation and the band projection generalizes easily to treat block banded form. Let M be the tensor product of two $N \times N$ matrices. Then we define 2D truncation as

$$\text{trunc}(M,\nu)_{ij} = \begin{cases} M_{ij}, & \text{if } 2\,|i-j-rN| \leq \nu - 1 - |2r| \\ 0, & \text{otherwise,} \end{cases} \quad |2r| + 1 \leq \nu. \tag{28}$$

For the band projection, the subspace is taken to be the space of matrices with the block banded sparsity pattern defined for two-dimensional truncation, (28), with the same requirement (18). In two dimensions, untangling the various H components from $\bar{L}$ is more complicated than finding the H for one-dimensional problems. There is however no unsurmountable difficulty, and truncating H instead of $\bar{L}$ can be done also for two-dimensional problems.

3 Elliptic Problems

In this section we present numerical results for the algorithms described above. We consider first the one-dimensional elliptic model equation,

$$-\frac{\partial}{\partial x}\left(a(x)\frac{\partial u}{\partial x}\right) = f(x), \qquad u(0) = u'(1) = 0, \tag{29}$$

and then the two-dimensional Helmholtz equation,

$$\nabla \cdot (a(x,y)\nabla u) + k^2 u = 0. \tag{30}$$

In both cases $a \geq \delta > 0$ for some positive δ. We use a uniform finite volume discretization in the numerical experiments. The computational domain will be the unit interval (square in 2D). The grid size will be denoted n, and the cell size $h = 1/n$. For a given function, $u(x)$, the corresponding grid function will be written u_i (or u_{ij}). The grid function approximates cell averages. For the whole vector $(u_1, \ldots, u_n)^T$ we will write U. In two dimensions, $U = (u_{11}, \ldots, u_{1n}, u_{21}, \ldots, u_{2n}, \ldots, u_{nn})^T$.

3.1 The elliptic model equation

We approximate (29) with the discretization

$$-\frac{1}{h^2}\Delta_+ a_i \Delta_- u_i = f_i, \qquad i = 1, \ldots, n, \qquad u_0 = -u_1, \qquad u_{n+1} = u_n. \tag{31}$$

First we set $f = -1$ and let the coefficients of $a(x)$ have a uniform random distribution in the interval $[0.5, 1]$. We take $n = 256$ and make three homogenization steps, i.e. the coarsest level contains 32 grid points.

In Figure 1 we compare different truncation strategies. In the top two subplots we use the truncation, as in [8]. In the bottom two subplots we use the band projection described in Section 2.3. The truncation is performed on H, see (10), and on $\bar{L}$ after all three homogenizations. We see that band projection gives a better approximation. We also see that it is more efficient to truncate H than to truncate $\bar{L}$. The exact reference solution here is the numerically homogenized solution at the coarsest level without any truncation. This is equivalent to the projection onto the coarse scale of the solution on the finest scale.

Next we change the coefficient in the differential equation to be

$$a(x) = \begin{cases} 1/6 & 0.45 < x < 0.55 \\ 1 & \text{otherwise.} \end{cases} \tag{32}$$

We keep all other characteristics. The result is given in Figure 2 and it shows that the relative merit of the different methods are just about the same.

The structure of the untruncated $\bar{L}$ matrices of the second example is shown at the left in Figure 3. The structure of H is similar. It should be noted that the local inhomogeneity of the full operator has spread out over a larger area, but it is still essentially local.

3.2 The Helmholtz equation

We now consider the two-dimensional Helmholtz equation, (30), with periodic boundary conditions in the y-direction, and $u(0, y) = 1$, $u_x(1, y) = 0$ at the left and right boundaries respectively. This corresponds to a plane time-harmonic wave of amplitude one entering the computational domain from the left and flowing out at the right. The discretization that we use is

$$\begin{aligned} -\frac{1}{h^2}\Delta_+^x a_{i\ell} \Delta_-^x u_{i\ell} - \frac{1}{h^2}\Delta_+^y a_{i\ell} \Delta_-^y u_{i\ell} - k^2 u_{i\ell} = 0, \qquad & i, \ell = 1, \ldots, n, \\ u_{i,0} = u_{i,n}, \quad u_{i,n+1} = u_{i,1}, \quad u_{n+1,\ell} = u_{n,\ell} \quad & u_{0,\ell} = 2 - u_{1,\ell}. \end{aligned} \tag{33}$$

This leads to the matrix equation

$$L_{j+1} U = F, \qquad U, F \in V_{j+1} \otimes V_{j+1}, \qquad n = m 2^{j+1}, \tag{34}$$

where m is a positive integer and L_{j+1} is homogenized using a tensor product extension of the theory in Section 2.1.

As an example we choose $a(x,y) = 10^{-4}$ when $0.4 < x < 0.5, |y - 0.5| > 0.05$ and 1 otherwise. This models a wall with a small slit where the incoming wave can pass through. With $k = 3\pi$ and $n = 48$, we obtained the results presented in Figure 4. In the same figure examples using truncation according to (28) is shown for various values of ν. The case $\nu = 9$ corresponds to a compression to approximately 7% of the original size. The structure of the operator after one homogenization step is shown in the middle of Figure 3.

4 Hyperbolic Problems

In this section we consider the time-dependent hyperbolic model equation in one space dimension,

$$\frac{\partial u}{\partial t} + a_\epsilon(x)\frac{\partial u}{\partial x} = f(x,t), \qquad u(0,t) = 0, \quad u(x,0) = g(x). \tag{35}$$

The variable coefficient $a_\epsilon(x)$ is positive and bounded.

The most straightforward way to homogenize (35) is by a semi-discrete approximation,

$$\frac{\partial u_i}{\partial t} + \frac{1}{h}a_i\Delta_- u_i = f_i(t), \qquad i = 1, \ldots, n, \qquad u_0 = -u_1, \quad u_i(0) = g_i, \tag{36}$$

with $a_i = a_\epsilon((i-1/2)h)$. In matrix form we will have

$$U_t + L_{j+1}U = F, \qquad n = 2^{j+1}, \tag{37}$$

which can be expressed in a wavelet basis as

$$\frac{\partial}{\partial t}\begin{bmatrix} U_h \\ U_l \end{bmatrix} + \begin{bmatrix} A_j & B_j \\ C_j & L_j \end{bmatrix}\begin{bmatrix} U_h \\ U_l \end{bmatrix} = \begin{bmatrix} F_h \\ F_l \end{bmatrix}, \quad U_h, F_h \in W_j, \quad U_l, F_l \in V_j. \tag{38}$$

We now claim that we can homogenize L_{j+1} in the same way as in the elliptic case, using the Schur complement. The motivation for this is (13), which shows that when the scales of $a_\epsilon(x)$ become very small, $\epsilon \to 0$, the effect of the time-derivative vanishes, $\frac{\partial}{\partial t}U_h \to 0$. As a limiting process in classical homogenization, this is fully justified, compare [3]. This argument implies that in the first set of equations of (38),

$$\frac{\partial U_h}{\partial t} + A_j U_h + B_j U_l = F_h \qquad \Rightarrow \qquad U_h = A_j^{-1}(-B_j U_l + F_h - \frac{\partial U_h}{\partial t}), \tag{39}$$

the last term, $-A_j^{-1}\frac{\partial}{\partial t}U_h$ is eliminated. Substitution into the second set of equations of (38) yields

$$\frac{\partial U_l}{\partial t} + \bar{L}_j U_l = \bar{F}_j, \tag{40}$$

with $\bar{L}_j$ and $\bar{F}_j$ defined by (6).

We found experimentally that using an approximation of the term $-A_j^{-1}\frac{\partial}{\partial t}U_h$ improved the homogenized operator. For the model problem (35) with $a_\epsilon = a(x/\epsilon)$ and $a(y)$ 1-periodic, we have, after a transient mode,

$$u_\epsilon(x,t) = \bar{u}(x,t) + \epsilon u_1(x, x/\epsilon, t) + \mathcal{O}(\epsilon^2), \tag{41}$$

compare [3]. Hence, $\frac{\partial^2}{\partial t^2}U_h$ is of the same order as $\frac{\partial}{\partial t}U_h$ since the oscillations on the ϵ-scale are not functions of time, and we here choose to neglect $-A_j^{-1}\frac{\partial^2}{\partial t^2}U_h$ instead of $-A_j^{-1}\frac{\partial}{\partial t}U_h$. Differentiation of (39) with respect to t gives the corrected homogenized operator $\tilde{L}_j$ and right hand side $\tilde{F}_j$,

$$\tilde{L}_j = K_j^{-1}\bar{L}_j, \qquad \tilde{F}_j = K_j^{-1}\bar{F}_j + K_j^{-1}C_jA_j^{-2}\frac{\partial F_h}{\partial t}, \qquad K_j = I + C_jA_j^{-2}B_j. \tag{42}$$

The corrected version of (40) has $\tilde{L}_j$, $\tilde{F}_j$ substituted for $\bar{L}_j$, $\bar{F}_j$ respectively. In principle, better approximations could be obtained by reiterating the steps above. After repeated differentiations of (39) we could choose to eliminate terms involving successively higher order time derivatives of U_h. However, the condition numbers of the correction matrices, K_j, produced in this manner rapidly deteriorate.

Let $n = 128$, $f \equiv 0$ and $g(x) = \sin^2(4\pi x)$ for $0 \le x \le 0.25$ and 0 otherwise. The result at time $t = 1$, is given in Figure 5 for the case of $a_\epsilon(x)$ uniformly random distributed in $[0.1, 2]$ and $a_\epsilon(x)$ as in (32). The effect of the first order correction is shown to the right. In these calculations, the time-integration was replaced by a fourth-order Runge-Kutta method.

Because of causality the full operator must be lower triangular in the hyperbolic case. The homogenized operator will keep this property and it can be written on the form $\bar{L} = H\Delta_-/h$. After two homogenization steps the operator, with $a_\epsilon(x)$ a slit, has the structure shown to the right in Figure 3. In view of this we approximate $\bar{L}$ and H, by truncation to lower triangular form. Like in the elliptic case, truncating the H matrix is more efficient than truncating $\bar{L}$.

5 Conclusions

The new technique of numerical homogenization based on wavelet projections, [8], has been improved and extended. The projection technique has been successfully applied to approximations of differential equations with local variations in the coefficients. This procedure can be seen as a systematic technique for subgrid scale modeling of general boundary value problems. After projection, a coarse grid operator is produced from a local fine grid representation. The coarse grid operator will represent the subgrid scale phenomena but otherwise have a structure similar to a coarse grid approximation of a homogeneous problem. This is useful for example when solving electromagnetic problems where fine geometry details might have large influence on the solution but can not be

resolved on a coarse grid. This approach has been tested in an example with the 2D Helmholtz equation.

A new truncation technique has been developed which increases the sparsity over the one described in [4]. The computational stencils of the new coarse grid operators are thus more compact.

The numerical homogenization technique does not apply directly to initial and initial boundary value problems. A new methodology has been developed which handles time dependent problems.

References

[1] J. Anderson. *Computational Fluid Dynamics, The Basics with Applications.* McGraw-Hill, 1995.

[2] O. Axelsson. *Iterative Solution Methods.* Cambridge University Press, 1994.

[3] A. Bensoussan, J.-L. Lions, and G. Papanicolau. *Asymptotic Analysis for Periodic Structures.* North-Holland Publ. Comp., The Netherlands, 1978.

[4] G. Beylkin, R. Coifman, and V. Rokhlin. Fast wavelet transforms and numerical algorithms I. *Comm. Pure Appl. Math.*, 44:141–183, 1991.

[5] M. Brewster and G. Beylkin. A multiresolution strategy for numerical homogenization. *Applied and Computational Harmonic Analysis*, 2:327–349, 1995.

[6] T. Chan and T. Mathew. The interface probing technique in domain decomposition. *SIAM J. Matrix Anal. Appl.*, 13(1):212–238, January 1992.

[7] I. Daubechies. *Ten Lectures on Wavelets.* SIAM, 1991.

[8] M. Dorobantu and B. Engquist. Wavelet-based numerical homogenization. *SIAM J. on Num. Anal.*, 35(2):540–559, April 1998.

[9] L. Durlofsky. Numerical calculation of equivalent grid block permeability tensors for heterogenuous porous media. *Water Resour. Res.*, 27:699–708, 1991.

[10] A. C. Gilbert. A comparison of multiresolution and classical one-dimensional homogenization schemes. *Appl. Comput. Harmon. Anal.*, 5(1):1–35, 1998.

[11] T. Y. Hou and X. H. Wu. A multiscale finite element method for elliptic problems in composite materials and porous media. *J. Comput. Phys.*, 134(1):169–189, 1997.

[12] S. Knapek. Matrix-dependent multigrid-homogenization for diffusion problems. *SIAM J. Sci. Stat. Comp.*, 1998. To appear.

[13] Z. Li. *The Immersed Interface Method—A Numerical Approach for Partial Differential Equations with Interfaces.* PhD thesis, Department of Applied Mathematics, Univ. of Washington, 1994.

[14] N. Neuss. *Homogenisierung und Mehrgitter.* PhD thesis, Fakultät Mathematik Universität Heidelberg, 1995.

[15] A. Taflove. *Computational Electromagnetics, The Finite-Difference Time-Domain Method*, chapter 10. Artech House, 1995.

[16] D. Wilcox. *Turbulence Modeling for CFD.* DCW Industries, Inc., 1993.

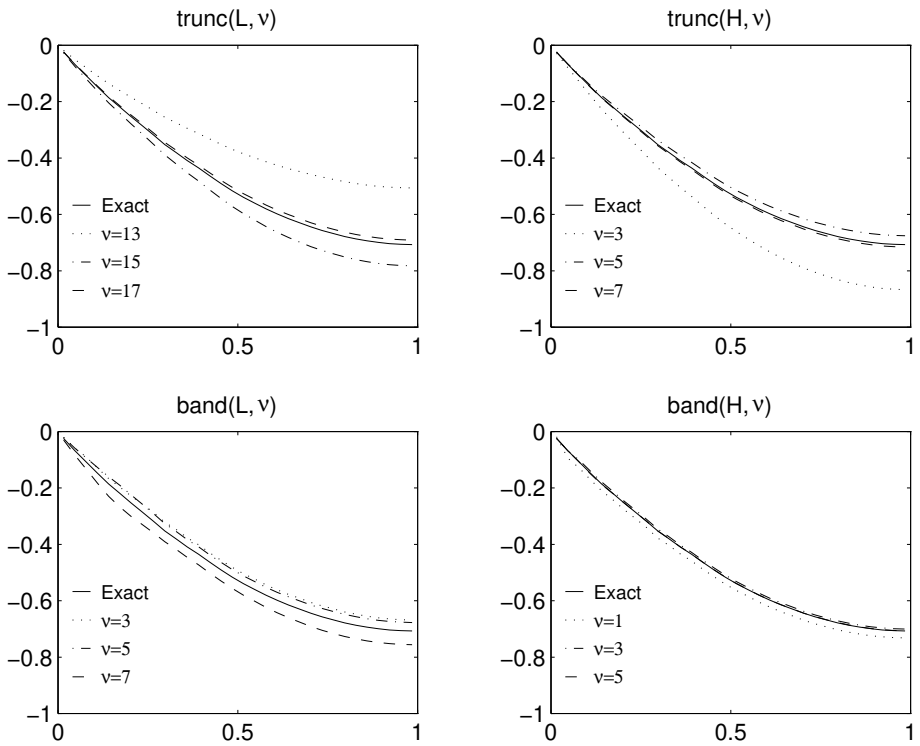

Figure 1: Result for the elliptic model problem, $a(x)$ random, when the homogenized operator is approximated in different ways. The "exact" solution refers to the solution with the full 32×32 homogenized operator.

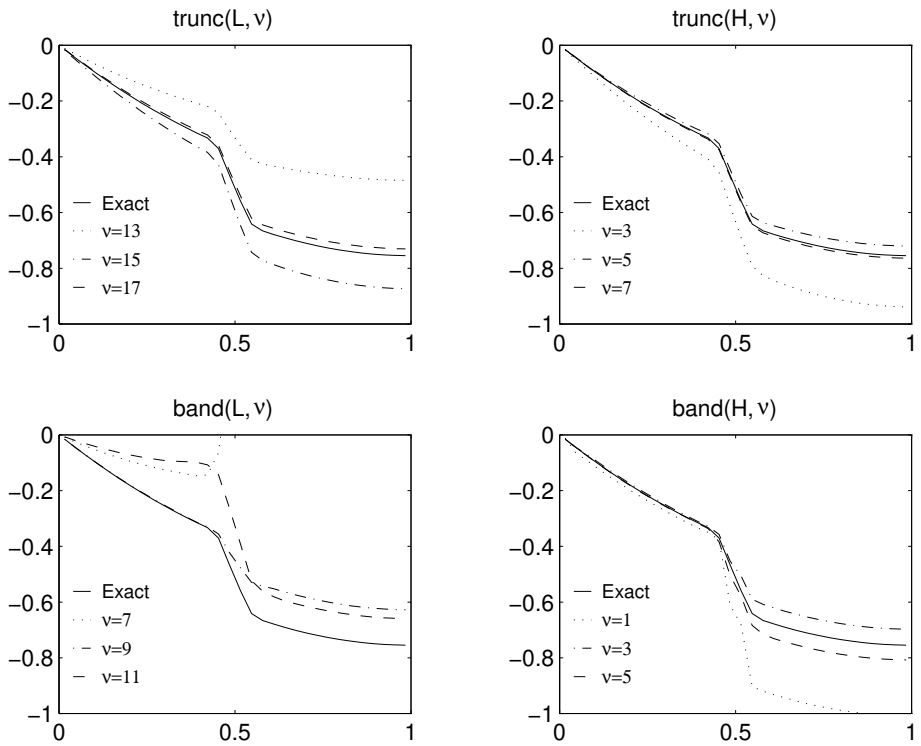

Figure 2: Result for the elliptic model problem, $a(x)$ a slit, when the homogenized operator is approximated in different ways. The "exact" solution refers to the solution with the full 32×32 homogenized operator.

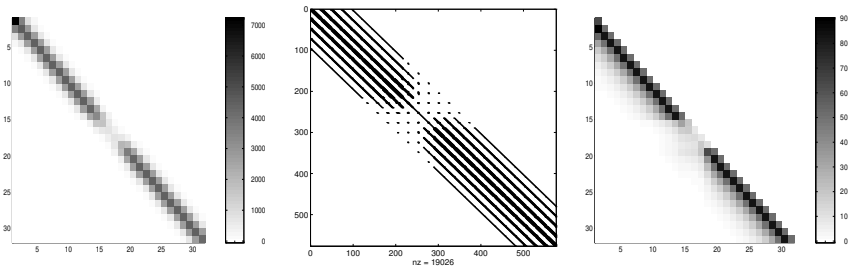

Figure 3: Structure of the untruncated homogenized operator $\bar{L}$ for three different cases: the elliptic model problem with $a(x)$ a slit (left), the 2D Helmholtz example (middle) and the hyperbolic problem with $a(x)$ a slit (right). Gray level indicates relative size of absolute value of element in left and right figures. Elements larger than 0.1% of max value shown in middle figure.

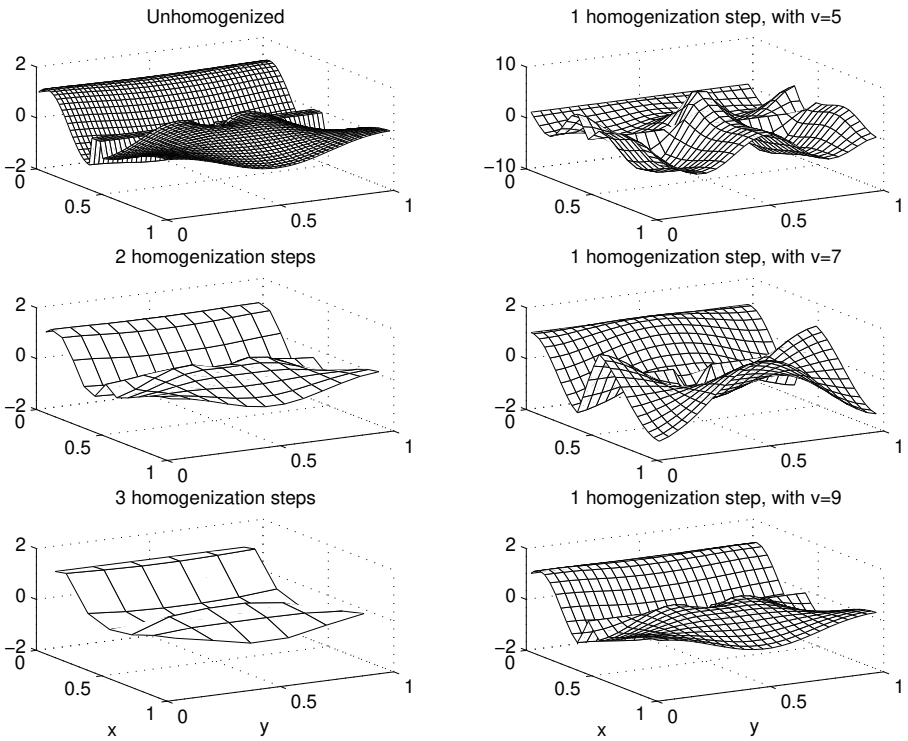

Figure 4: Result for the 2D Helmholtz example. Left column shows solution using the untruncated homogenized operator after $0, 2, 3$ homogenization steps. Right column shows solution using the one step homogenized operator, truncated with different ν.

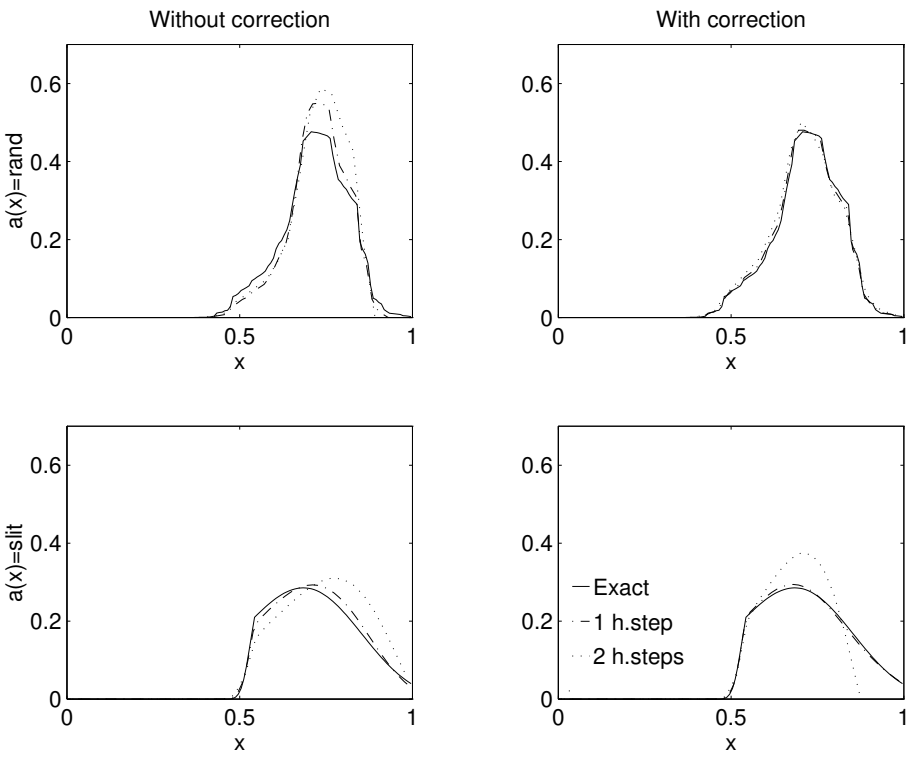

Figure 5: The solution $u(x)$ at $t = 1$ for the hyperbolic case, using different $a_\epsilon(x)$, with and without first order correction. Solutions shown are the exact solution, computed with the full operator, and solutions computed with the operator homogenized one and two steps.